CMS Physics Analysis Summary

Contact: cms-pag-conveners-b2g@cern.ch 2017/12/08

Search for heavy resonances decaying into two Higgs bosons or into a Higgs and a vector boson in proton-proton collisions at 13 TeV

The CMS Collaboration

Abstract

A search is presented for massive resonances decaying either into two Higgs (H) bosons or into a Higgs and a vector (V = W or Z) boson. The decay channels considered are VH $\to q\bar{q}\tau^+\tau^-$ and HH $\to b\bar{b}\tau^+\tau^-$. This analysis is based on the data sample of proton-proton collisions collected at a center-of-mass energy of 13 TeV by the CMS Collaboration in 2016, corresponding to an integrated luminosity of 35.9 fb^{-1}. For the high-mass resonances considered ($\gtrsim$ 1 TeV), substructure techniques are employed to differentiate between the hadronization products of a vector boson decaying to quarks, a Higgs boson decaying to bottom quarks, and quark- or gluon-induced jets. Due to the large boost of the Higgs boson, the two leptons in the $H \to \tau^+\tau^-$ decay are collimated. Advanced techniques are used for events in which one τ lepton decays hadronically and the other leptonically, and in which both decay hadronically. Upper limits at 95% confidence level are set on the product of cross section times branching fraction for resonance masses between 900 and 4000 GeV, ranging from 100 to 6 fb for spin 0 and 2 resonances, and from 250 to 6 fb for spin 1 resonances.

1 Introduction

Heavy resonances that decay to VV, VH, or HH, where V denotes a W or Z boson and H the Higgs boson, are motivated by theories beyond the standard model (SM) that address the large difference between the electroweak and gravitational scales. These heavy particles arise as Kaluza-Klein (KK) excitations of spin-0 radions [1–3], as well as spin-2 gravitons predicted by models based on Randall-Sundrum warped extra dimensions [4, 5] with the gravitons propagating in the bulk [6–8]. Heavy spin-1 W′ and Z′ particles that decay to VV and VH are postulated in composite Higgs models [9–12], little Higgs models [13, 14], and in the sequential standard model (SSM) [15]. These models are generalized in the heavy vector triplet (HVT) framework [16]. These new hypothetical particles with spins of 0, 1, or 2 can be produced at the CERN LHC, as depicted in the diagrams of Fig. 1.

The bulk graviton model is described by two free parameters: the mass of the first KK excitation of the spin-2 boson, denoted as the KK bulk graviton, and the ratio $\tilde{k} \equiv k/\overline{M}_{\mathrm{Pl}}$, where k is the unknown curvature scale of the extra dimension and $\overline{M}_{\mathrm{Pl}} \equiv M_{Pl}/\sqrt{8\pi}$ is the reduced Planck mass. Searches for radions in this model can be described in terms of the radion mass and the ultraviolet mass scale of the theory, Λ_R [17]. The HVT model is described in terms of four parameters: the mass of the new vector bosons, their coupling strength to fermions c_{F}, the coupling strength to the Higgs boson and longitudinally-polarized SM vector bosons c_{H}, and the strength of the new vector boson interaction g_{V}. Searches for diboson resonances have previously been performed in several final states, placing lower limits on the masses of these resonances above the TeV scale [18–30].

This paper presents a search for resonances with masses above 900 GeV decaying into VH or HH. The analysis is based on proton-proton collision data collected at $\sqrt{s} = 13$ TeV by the CMS experiment at the CERN LHC during 2016, and corresponding to an integrated luminosity of 35.9 fb^{-1}. The final states considered are VH $\to \mathrm{q\bar{q}}\tau^+\tau^-$ and HH $\to \mathrm{b\bar{b}}\tau^+\tau^-$. Events are classified as "semi-leptonic", denoted as $\ell\tau_h$, if one τ lepton decays leptonically (ℓ) into a muon or an electron and the other decays hadronically (τ_h); and "fully-hadronic", denoted as $\tau_h\tau_h$, if both τ leptons decay hadronically. The analysis aims to reconstruct the diboson decay products in order to search for a local enhancement in the diboson invariant mass spectrum.

Since the resonances under study have masses of $\mathcal{O}$(TeV), the bosons they decay into typically have transverse momenta of at least several hundred GeV. As a consequence, the decay products are collimated such that the hadronically decaying bosons cannot be resolved by standard jet algorithms. Dedicated techniques, called V tagging and H tagging, are applied to exploit the substructure of these large-cone jet objects in order to resolve the hadronically decaying V and H bosons. For the Higgs boson decaying to a pair of τ leptons, the decay products are also close in angular separation. The τ reconstruction and identification techniques elaborated in Ref. [25] are adopted for an optimal signal significance in this peculiar event topology.

2 The CMS detector

The central feature of the CMS apparatus is a superconducting solenoid of 6 m internal diameter, providing a magnetic field of 3.8 T. Within the solenoid volume are a silicon pixel and strip tracker, a lead tungstate crystal electromagnetic calorimeter (ECAL), and a brass and scintillator hadron calorimeter (HCAL), each composed of a barrel and two endcap sections. Forward calorimeters extend the pseudorapidity coverage provided by the barrel and endcap detectors. Muons are measured in gas-ionization detectors embedded in the steel flux-return yoke outside the solenoid. The CMS two-level trigger system [31] reduces the event rate from the bunch

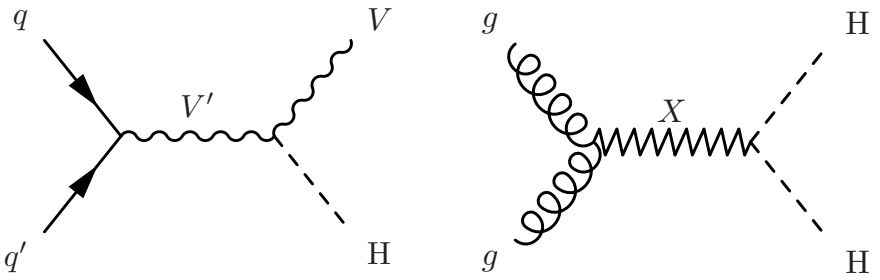

Figure 1: Feynman diagrams for the production of a heavy vector boson V′ (W′ or Z′) that decays to a vector boson and a Higgs boson (left) and the production of a spin-0 radion or a spin-2 graviton that decays to a Higgs boson pair (right).

crossing rate of 40 MHz down to less than 1 kHz of data to be stored.

A more detailed description of the CMS detector, together with a definition of the coordinate system used and the relevant kinematic variables, can be found in Ref. [32].

3 Data sample and simulation

The data sample analyzed in this search corresponds to an integrated luminosity of 35.9 fb^{-1}, collected in proton-proton collisions with the CMS detector during the 2016 data taking period. The signal processes $\text{pp} \to \text{X} \to \text{VH} \to \text{q}\bar{\text{q}}\tau^+\tau^-$ and $\text{pp} \to \text{X} \to \text{HH} \to \text{b}\bar{\text{b}}\tau^+\tau^-$ are simulated at leading order (LO) using the MADGRAPH5_aMC@NLO v2.2.2 [33] Monte Carlo (MC) event generator. The natural width of the resonance is assumed to be smaller than the experimental resolution of its reconstructed mass, as verified in the benchmark scenarios considered for the radion and HVT models.

Standard Model background processes are generated using MC simulation. The MADGRAPH5_aMC@NLO generator at LO is used to describe events with Z/γ+jets and W+jets production. The POWHEG v2 generator is used to simulate $\text{t}\bar{\text{t}}$ and single top quark production at next-to-leading order (NLO) [34–37]. The PYTHIA 8.205 [38] generator at LO is used for SM diboson and QCD multijet events. For all signal and background samples, showering and hadronization are described using PYTHIA, τ lepton decays are described using TAUOLA 1.1.5 [39], and the response of the detector is described using GEANT4 [40]. Additional collisions in the same or adjacent bunch crossings (pileup) are taken into account by superimposing minimum bias interactions onto the hard scattering processes, with a frequency distribution matching the one observed.

4 Event reconstruction

The particle-flow (PF) event algorithm [41] reconstructs and identifies each individual particle with an optimized combination of information from the various elements of the CMS detector. The energy of electrons is determined from a combination of the electron momentum at the primary interaction vertex as determined by the tracker, the energy of the corresponding ECAL cluster, and the energy sum of all bremsstrahlung photons spatially compatible with originating from the electron track. The energy of muons is obtained from the curvature of the corresponding track. The energy of charged hadrons is determined from a combination of their momentum measured in the tracker and the matching ECAL and HCAL energy deposits, corrected for zero-suppression effects and for the response function of the calorimeters to hadronic showers. Finally, the energy of neutral hadrons is obtained from the corresponding corrected

ECAL and HCAL energies.

The identified particles are clustered into jets using the anti-k_T algorithm [42], implemented in the FASTJET package [43]. Two different distance parameters are used, $R = 0.4$ and $R = 0.8$, referred to as AK4 and AK8 jets, respectively. AK4 jets are used primarily to reject or select events with top quarks, while the larger AK8 jets are used to identify and contain hadronically decaying W, Z and Higgs boson candidates. The charged hadron subtraction (CHS) pileup mitigation algorithm discards charged particles not originating from the primary vertex, defined as the one with the highest sum of the p_T^2 of the physics objects. The physics objects are the jets, clustered with the tracks assigned to the vertex as inputs to the jet finding algorithm, and the associated missing transverse momentum, taken as the negative vector sum of the p_T of those jets. The residual contamination from neutral pileup particles is estimated to be proportional to the event energy density and the jet area, and is removed from the jet energy calculation. Jet momentum is determined as the vectorial sum of all particle momenta in the jet, and is found from simulation to be within 5 to 10% of the true momentum over the entire p_T spectrum and detector acceptance. Jet energy corrections are derived from simulation, and are confirmed with in situ measurements of the energy balance in dijet and γ+jets events. Additional selection criteria are applied to each event to remove spurious jet-like features originating from isolated noise patterns in certain HCAL regions. The AK4 and AK8 jets must have $p_T > 20\,\text{GeV}$ and 200 GeV, respectively, and $|\eta| < 2.4$ to be considered in the subsequent steps of the analysis.

To determine the mass of the jet and the values of the substructure variables used to identify hadronic decays of the bosons, the so-called pileup per particle identification (PUPPI) algorithm [44] is applied to AK8 jets instead of CHS. The PUPPI algorithm uses local shape information, event pileup properties, and tracking information together in order to compute a weight describing the likelihood for each particle to originate from a pileup interaction. The weight is used to rescale the particle four-momenta, superseding the need for further jet-based corrections. The PUPPI constituents are subsequently clustered with the same algorithm used for CHS jets, and then matched to the AK8 jets clustered with the CHS constituents, which are used for the kinematic selection.

Subsequently, the soft-drop algorithm [45, 46], designed to remove contributions from soft radiation, is applied to the AK8 PUPPI jets. The soft drop jet mass m_j is defined as the invariant mass associated with the four-momentum of the soft drop jet. Dedicated mass corrections, derived from data in a region enriched with $\mathrm{t\bar{t}}$ events containing merged $\mathrm{W(q\bar{q})}$ decays, are applied to m_j, to remove any dependence on the jet p_T and to match the jet mass and resolution observed in data.

The two-prong decay of massive W and Z boson candidates is used to discriminate against jets initiated from quarks and gluons. The constituents of the jet are clustered again with the k_T algorithm, and the procedure is stopped when N subjets are obtained. Subsequently, the N-subjettiness as defined in Ref. [47] is calculated on the PUPPI-corrected jet for the one and two subjet hypothesis as

$$\tau_N = \frac{1}{d_0} \sum_k p_{T,k} min(\Delta R_{1,k}, \Delta R_{2,k}, \ldots, \Delta R_{N,k}). \quad (1)$$

The normalization factor is $d_0 = \sum_k p_{T,k} R_0$, where R_0 is the radius of the original jet, the index k increments over the jet constituents, and $\Delta R_{N,k}$ are the angular distances defined for two particles as $\Delta R = \sqrt{(\Delta\eta)^2 + (\Delta\phi)^2}$, and calculated here with respect to the axis of the N^{th} subjet. For the ratio of 2-subjettiness to 1-subjettiness, $\tau_{21} = \tau_2/\tau_1$, small values correspond to

a high compatibility with the hypothesis of a massive object decaying into two partons. The efficiency of the τ_{21} selection is measured from data in a $\bar{\mathrm{t}}\mathrm{t}$ enriched sample [48].

Jets originating from a Higgs boson candidate are likely to have two displaced vertices due to the long lifetime and large mass of the b quarks that are the dominant decay mode. Following the procedure above, jet clustering with the k_{T} algorithm is performed and stopped when two subjets are identified. The inclusive combined secondary vertex b tagging algorithm [49, 50] is applied to the two subjets, which are considered as b tagged if they pass a working point that provides a misidentification rate of ≈10% while maintaining high efficiency. In order to remove backgrounds containing top quark decays, AK4 jets found in the event that do not overlap with the AK8 jet are subjected to a veto based on the same b tagging algorithm, but with an efficiency of ≈70% for identifying B hadrons and a ≈1% misidentification rate. The ratio of the b tagging efficiency from data compared to simulation is used as a scale factor to correct the simulated events.

A dedicated reconstruction algorithm is used to reconstruct the Higgs boson decaying to τ leptons [51]. Higgs boson candidates decaying to τ leptons are clustered using the Cambridge-Aachen algorithm [52] with a cut-off parameter of $R = 0.8$ (CA8 jets). For each CA8 jet with $p_{\mathrm{T}} > 100\,\mathrm{GeV}$, the last step of the clustering is undone iteratively until the two resulting subjets are found to have $p_{\mathrm{T}} > 10\,\mathrm{GeV}$ and satisfy the mass drop condition which is that $\max(m_{\mathrm{subjet1}}, m_{\mathrm{subjet2}})/m_{\mathrm{CA8jet}} < 2/3$. If these conditions are met, the two subjets are used as seeds in the standard τ reconstruction and the hadron plus strip algorithm [53] is applied on them to identify hadronic taus, otherwise, the unclustering procedure is repeated for the most energetic subjet. The τ leptons selected by the hadron plus strip algorithm are then required to have $|\eta| < 2.3$ and $p_{\mathrm{T}} > 20\,\mathrm{GeV}$ and satisfy a multivariate (MVA) τ-ID isolation discriminator, which is the output of a boosted decision tree. This is trained to discriminate between real hadronic taus and hadronic jets using variables related to energy deposits and track impact parameters that are correlated to the tau lepton lifetime. A medium working point is used for the leading tau and a very loose one is used for the second leading tau in fully hadronic events.

Electrons are reconstructed in the region $|\eta| < 2.5$ by matching energy deposits in the ECAL with tracks reconstructed in the tracker [54]. The electron identification is based on the distribution of energy deposited along the electron trajectory and the direction and momentum of the track in the inner tracker. Additional requirements are applied to remove electrons produced by photon conversions. Electrons are further required to be isolated from other activity in the detector. The electron isolation parameter is defined as the sum of transverse momenta of all the PF candidates (excluding the electron itself) within $\Delta R < 0.3$ around the electron direction, after the contributions from pileup and particles associated with reconstructed hadronic taus within the isolation cone are removed.

Muons are reconstructed within the acceptance of the CMS muon system, $|\eta| < 2.4$, using information from both the muon spectrometer and the silicon tracker [55]. Muon candidates are identified based on the compatibility of tracks reconstructed from only the silicon tracker as compared with tracks reconstructed from the combination of hits in both the tracker and the muon detector. Additionally, the trajectory is required to be compatible with the primary vertex, and have a sufficient number of hits in the tracker and muon systems. Muons are required to be isolated from reconstructed tracks within a cone $\Delta R < 0.4$ around the muon direction that are not associated with the muon or reconstructed hadronic tau decay products.

The missing transverse momentum vector $\vec{p}_{\mathrm{T}}^{\,\mathrm{miss}}$ is defined as the negative vectorial sum of the momenta of all PF candidates projection onto the plane perpendiculate to the beam direction. The missing hadronic activity $H_{\mathrm{T}}^{\mathrm{miss}}$ is defined as the magnitude of the negative vectorial sum

of the transverse momenta of all AK4 jets with $p_T > 30\,\text{GeV}$.

5 Event selection

Events are selected using a set of triggers that require a missing transverse momentum value as low as 90 GeV. The low p_T^{miss} threshold is achieved by combining it with additional requirements such as the presence of a jet with $p_T > 80\,\text{GeV}$, or a significant imbalance of hadronic transverse momentum, H_T^{miss}. The efficiency of the trigger is measured on an independent sample selected with muon triggers, and after applying the offline event selection, is verified to be above 95% with an uncertainty of about 2%.

All events in this analysis are required to contain one Higgs boson candidate decaying to $\ell\tau_h$ or $\tau_h\tau_h$. The other boson candidate is hadronically-decaying and reconstructed as a jet with the same kinematic criteria in all categories. Its soft drop jet mass must be in the interval 65–135 GeV. If the mass is in the range 65–85 GeV, the boson is consistent with a W boson, while the range 85–105 GeV is consistent with a Z boson, and the range 105–135 GeV with a Higgs boson. In order to discriminate against backgrounds, the hadronic W or Z bosons decays are required to have small values of τ_{21} and events are divided into a high purity (HP) category if $\tau_{21} < 0.4$, and a low purity (LP) category with $0.4 < \tau_{21} < 0.75$. The normalization scale factors 0.99 ± 0.06 for the high purity region and 0.96 ± 0.11 for the low purity region [48] are applied to simulated events with genuine hadronic boson decays. Higgs-boson jet candidates are classified according to the number of subjets (1 or 2) that pass the b tagging selection. Subjet b tagging is not used for jets compatible with W or Z candidates and no N-subjettiness requirement is applied to the hadronic Higgs candidate jet. If neither the N-subjettiness nor the b-tagging requirements are satisfied, the event is discarded.

Events are divided into categories depending on the number of hadronic taus (1 or 2) identified, and on the classification of the large jet cone: either high purity or low purity in τ_{21}, or either 1 or 2 b tagged subjets.

Since the undetected neutrinos carry a significant fraction of the di-tau system momentum, signal events are expected to have a large missing transverse momentum, justifying the use of triggers that require large p_T^{miss} or H_T^{miss}. A stringent offline selection of greater than 200 GeV is applied on the reconstructed p_T^{miss}, in order to ensure a stable trigger efficiency and to suppress the background contribution from QCD multijet events. Events with top quark pairs and single top quarks are suppressed by removing events in which any AK4 jet is b tagged.

Several selection requirements are applied to remove backgrounds with low-mass SM resonances and containing overlaps between the lepton and tau lepton reconstruction in the detector. The angular distance $\Delta R_{\tau,\tau}$ should be greater than 0.05, where $\Delta R = \sqrt{(\Delta\eta)^2 + (\Delta\phi)^2}$, and the di-tau mass should be between 50 and 150 GeV, as estimated from the SVFit procedure [56]. Additionally, an upper cut is placed on $\Delta R_{\tau,\tau}$ of 1.5 in order to reject W+jets events, in which a jet misidentified as a tau lepton is usually well-separated in space from the isolated lepton.

6 Background estimation

The main sources of background events originate from top quark pair production and from the production of a vector boson in association with jets (Z+jets and W+jets), while minor contributions come from single top quark, diboson, and multijet production. In the background estimation procedure, the background contributions are split in two: top quark pair and sin-

gle top quark production, and V+jets, which accounts for Z+jets and W+jets, multijet, and SM diboson production.

The normalization of the top quark pair and single top quark background is determined in dedicated control regions enriched in top quark events. Control regions with a high purity of top quark events are found by inverting the b tag veto on the AK4 jets and further tightening the b tag selection. Events are separated according to the lepton flavour and the requirements on the large-cone jet identification. Data are found to be described well by simulations in terms of the jet and di-jet resonance mass distributions. Multiplicative scale factors are determined in order to correct for the difference in the normalization between data and simulation in the control regions, after subtracting the other background contributions. Scale factors, derived in the semileptonic control regions, are applied also to the fully hadronic channel, where the statistics are lower. The normalization of top quark pair and single top quark processes in each region is corrected with the use of scale factors, which are reported in Table 1, and depend on the selection applied on the large cone jet for a given category.

Table 1: Normalization scale factors for top quark production for different event categories. Uncertainties are due to the limited size of data statistics in the control regions and the uncertainty on the b tagging efficiency.

Channel	τ_{21} LP	τ_{21} HP	1 b-tagged subjet	2 b-tagged subjets
$\ell\tau_h$	0.96 ± 0.04	1.06 ± 0.06	1.00 ± 0.06	1.11 ± 0.15

The estimation of the contribution of the V+jets background is based on data, in regions defined by applying the full signal region selection except the jet mass requirements. Data are divided into the fully hadronic ($\tau_h\tau_h$) and the semileptonic ($\ell\tau_h$) channels. Two jet-mass sidebands (SBs) are defined with jet masses in the range 30–65 GeV for the low sideband (LSB), or above 135 GeV for the high sideband (HSB), and used to predict the background contribution in the signal region (SR). Analytic functions are fit to the simulated distributions of the jet mass, considering separate shapes for V+jets and top quark production. The normalization of the V+jets background is extracted by fitting the data with the sum of all contributing background processes in the jet mass sidebands, after fixing all the non V+jets processes shape and normalizations, as shown in Fig. 2 for the HP τ_{21} category of semileptonic events.

The procedure is repeated with an alternative function for the V+jets jet mass modeling and the difference in the normalization is considered as a systematic uncertainty. The expected number of background events in each signal region is reported in Table 2.

The simulated resonance mass distributions are fit in the sideband and signal regions with analytic functions in order to determine the expected background shapes. The shape of the resonance mass (m_X) for the V+jets background in the signal region is determined through the use of a transfer function, determined from simulations as

$$\alpha(m_X) = \frac{N_{SR}^{MC,bkg}(m_X)}{N_{SB}^{MC,bkg}(m_X)} \tag{2}$$

where $N_{SR}^{MC,bkg}(m_X)$ and $N_{SB}^{MC,bkg}(m_X)$ are probability distribution functions that model the simulated resonance mass in the SR and SBs. Then the shape of the V+jet background in the SR is extracted from data events in the sideband, after subtracting the top background estimated by simulation, and multiplying by the $\alpha(m_X)$ transfer function. The resonance mass distribution

Table 2: Predicted number of background events and observed number of events in the signal region, for all event categories. W, Z and H regions are intervals in the jet softdrop mass distribution that range from 65 GeV to 85 GeV, from 85 GeV to 105 GeV, and from 105 GeV to 135 GeV respectively. Separate sources of uncertainty in the expected number are reported: the statistical uncertainty on the V+jet contribution from the fit procedure (fit), the one due to the difference between the nominal and alternative function chosen for the fit (alt), and the top background uncertainty from the fit to the simulated jet mass spectrum.

Category			V+jets ($\pm$ fit)($\pm$ alt)	Top	Total exp. events	Obs. events
W region	HP	$\ell\tau_h$	$37.9 \pm 6.5 \pm 12.2$	37.8 ± 0.6	75.7 ± 13.8	78
		$\tau_h\tau_h$	$13.0 \pm 3.2 \pm 0.2$	16.0 ± 1.8	29.0 ± 3.7	45
	LP	$\ell\tau_h$	$105.3 \pm 6.8 \pm 9.0$	34.2 ± 0.9	139.5 ± 11.4	120
		$\tau_h\tau_h$	$27.0 \pm 3.3 \pm 3.0$	12.3 ± 0.6	39.3 ± 4.5	37
Z region	HP	$\ell\tau_h$	$39.9 \pm 6.1 \pm 7.9$	42.4 ± 1.0	82.3 ± 10.0	82
		$\tau_h\tau_h$	$13.7 \pm 3.0 \pm 2.5$	18.0 ± 1.8	31.6 ± 4.3	33
	LP	$\ell\tau_h$	$73.5 \pm 4.8 \pm 6.1$	29.1 ± 1.9	102.6 ± 8.0	92
		$\tau_h\tau_h$	$19.1 \pm 2.3 \pm 2.5$	10.4 ± 0.8	29.5 ± 3.5	33
H region	2 b-tag	$\ell\tau_h$	$2.4 \pm 0.9 \pm 0.4$	6.9 ± 0.6	9.2 ± 1.2	10
		$\tau_h\tau_h$	$1.1 \pm 0.6 \pm 0.0$	3.8 ± 1.8	4.9 ± 1.9	5
	1 b-tag	$\ell\tau_h$	$29.3 \pm 3.5 \pm 6.6$	37.3 ± 1.2	66.6 ± 7.5	56
		$\tau_h\tau_h$	$11.5 \pm 2.2 \pm 2.6$	15.4 ± 1.7	26.9 ± 3.8	23

is shown in Fig.2 for semileptonic τ_{21} HP events. The ratio $\alpha(m_X)$ accounts for the small kinematical differences and the correlations involved in the interpolation from the sideband to the signal region.

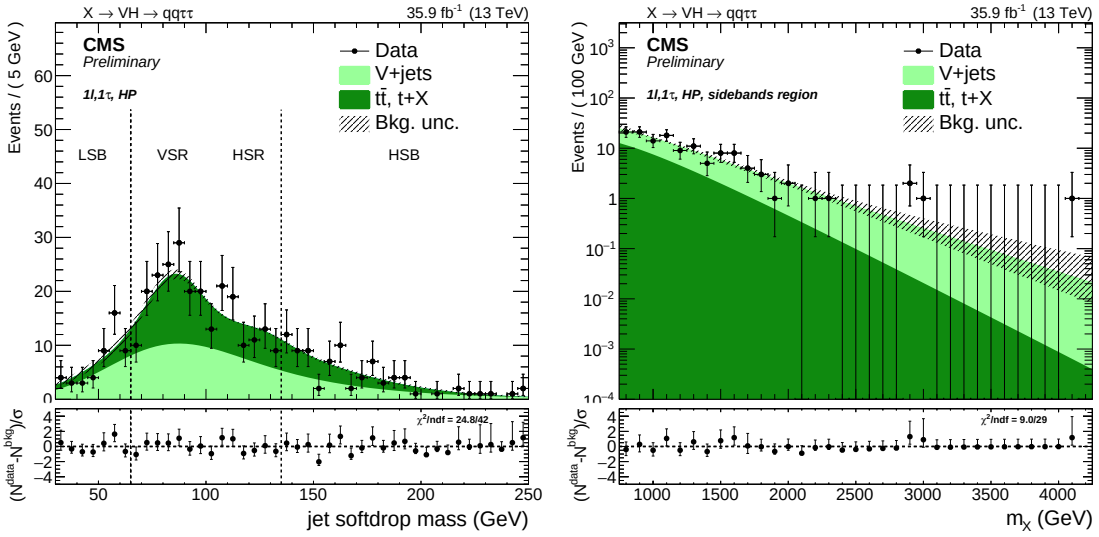

Figure 2: Fit to data for the τ_{21} HP $\ell\tau_h$ channel of the softdrop mass distribution in order to determine the background normalization (left) and to the resonance mass spectrum in order to determine the background shape in the sidebands (right).

The overall background predicted in the SR is then:

$$N_{SR}^{data}(m_X) = \alpha(m_X) \times [N_{SB}^{data} - N_{SB}^{Top}](m_X) + N_{SR}^{Top}(m_X) \quad (3)$$

where N_{SB}^{Top} and N_{SR}^{Top} are the background distributions for top quark events fixed to the shape

and normalizations derived from the yields expected from simulation corrected by the scale factors 1. The distributions of expected backgrounds in the signals regions are reported in Figs. 3–4.

7 Systematic uncertainties

The systematic uncertainty in the determination of the V+jets background yield is dominated by the statistical uncertainty associated with the amount of events in the jet mass sidebands in data and simulation. An additional uncertainty is related to the choice of the jet mass modeling used for the V+jets background estimation and it is evaluated by using the alternative functions in the background estimation and considering the difference in the expected yields as a systematic uncertainty. For the top quark processes, normalization and shape uncertainties from the parametrization are propagated to the final background estimation. The single top quark and top quark pair production normalization uncertainty comes predominantly from the number of events in the control regions.

The V+jets shape uncertainties are estimated from the covariance matrix of the fit to m_X in the sidebands and the uncertainties of the $\alpha(m_X)$ ratio that depend on the number of events in data and simulation, respectively.

The uncertainties on the trigger efficiency, and the electron and muon reconstruction, identification and isolation efficiencies each amount to 1–2%. For the τ lepton reconstruction and identification the uncertainties vary between 6% (10%) and 8% (13%) depending on the resonance mass in the semileptonic (fully hadronic) channel. A separate uncertainty due to the extrapolation of the reconstruction and identification of tau leptons at large p_{T} is estimated to be 18% in the semileptonic and 30% in the fully hadronic channels for a 4 TeV signal mass hypothesis. This contributes to an increase of 1% in the width of the signal shapes.

Jet energy scale and resolution uncertainties affect both selection efficiencies and shape. The corrections to the jet mass scale and resolution are also taken into account and result in a variation of 1–8% for the expected signal events. The jet energy scale accounts for a variation of 1–3%, while the variation of the jet energy resolution has an impact of 1–2% on the signal efficiency. The effect on the mass distribution of the resonance are a variation of 1–2 % on the mean and the width of the signal shapes. Event migrations between the mass windows due to jet mass scale and resolution variation are quantified between 2 and 15% depending on the signal and the vector boson mass region.

Scale factors for W tagging and b tagging represent the largest source of normalization uncertainty for the signal. For signal events, W tagging normalization uncertainties amount to 6% (11%) in the HP (LP) categories. An additional uncertainty due to the extrapolation of the V jet tagging from the $t\bar{t}$ scale to larger jet p_{T} is estimated using an alternative HERWIG [57] shower model, and varies from 2 to 18% between the 1 and 4 TeV mass hypotheses and W-tagging categories. Furthermore, the impact due to the uncertainty of b tagging varies between 3% (4%) and 7% (5%) for the 2 b-tagged subjet (1 b-tagged subjet) categories.

Tau energy scale uncertainties affect both selection efficiencies and shape. The normalization difference is 1% in the semileptonic channel, while it varies from 5 to 3% between the 1 and 4 TeV mass hypotheses.

Normalization uncertainties due to the choice of PDF grow larger with higher resonance mass, and are larger for gluon-intiated processes with respect to quark-initiated ones. For W′ and Z′ production, which are sensitive to quark PDFs, effects range from 6 to 37%, while Radion and

Graviton production depends on gluon PDFs, and results in a variation from 10 to 64% on the number of signal events expected. Uncertainties of similar magnitude arise from the variation of the factorization and renormalization scale, which are ranging from 3 to 13% for W′ and Z′, and from 10 to 19% for Radion and Graviton production. While normalization uncertainties are not accounted for in the limit setting, effects on the signal acceptance are propagated to the final fit amounting to 0.5–2% for the PDF uncertainties, depending on the resonance mass.

Further systematic uncertainties affecting the normalization of signal and minor backgrounds considered in the analysis include pileup contributions (0.5%) and integrated luminosity (2.6%). A list of the main systematic uncertainty contributions is reported in Table 3.

Table 3: Summary of systematic uncertainties for the background and signal samples. Uncertainties marked with † are not included in the limit bands, but instead reported in the theory band.

	shape	V+jets	$t\bar{t}$, t+X	Signal
α-function	✓	✓	-	-
Bkg. normalization		11–60%	2–38%	-
Top scale factors		-	5–14%	-
jet energy scale	✓	-	-	✓
jet energy resolution	✓	-	-	✓
jet mass scale		-	-	1%
jet mass resolution		-	-	8%
V tagging		-	-	6%(HP)–11%(LP)
V tagging extr.		-	-	8%–18%(HP), 2%–8%(LP)
b-tagging		-	-	3–7% (1b), 3.7–5.4% (2b)
b-tagged jet veto		-	3%	1%
trigger		-	-	2%
leptons Id, Iso		-	-	2%
τ Id		-	-	6–8% ($\ell\tau_h$), 10–13% ($\tau_h\tau_h$)
τ Id pt extr.	✓	-	-	0.5–18% ($\ell\tau_h$), 0.2–30% ($\tau_h\tau_h$)
τ energy scale	✓	-	-	1% ($\ell\tau_h$), $5-3$% (τ_h)
pile-up		-	-	0.5%
QCD scales†		-	-	2.5%–12.5%, 10%–19%
PDF scale†		-	-	6%–37% ,10%–64%
PDF acceptance		-	-	0.5%–2%
luminosity		-	-	2.6%

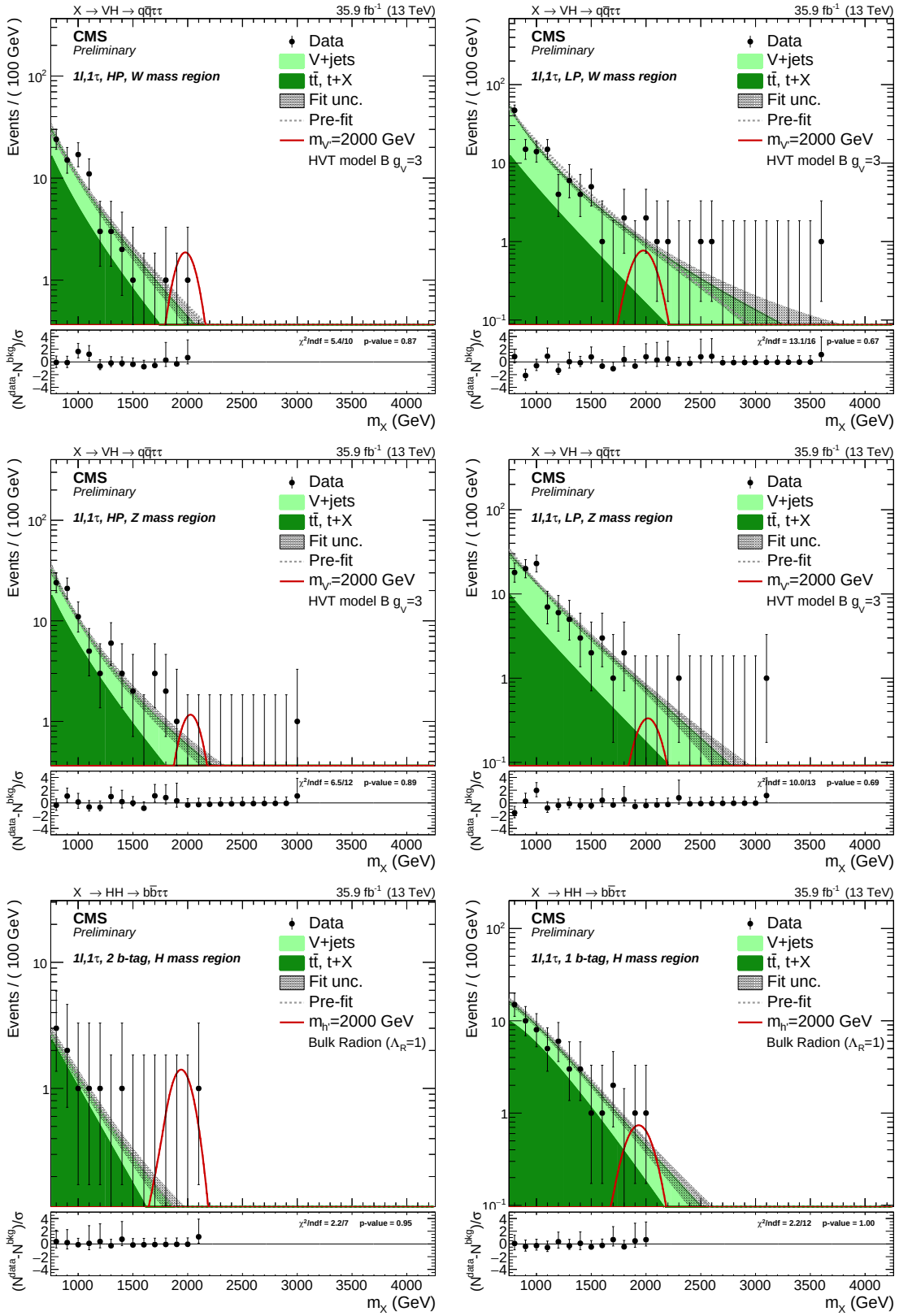

Figure 3: Data and expected backgrounds determined with the α transfer function method in the $\ell\tau_h$ channel: W mass window for the τ_{21} HP (upper left) and LP (upper right) categories, Z mass window for the τ_{21} HP (middle left) and LP (middle right) categories, and H mass window for the 1 b tagged subjet (lower left) and 2 b tagged subjets (lower right) categories.Signal contributions are also shown assuming the benchmark scenario B of the HVT model for the V′ and Λ_R=1 for the radion, each with a mass of 2 TeV.

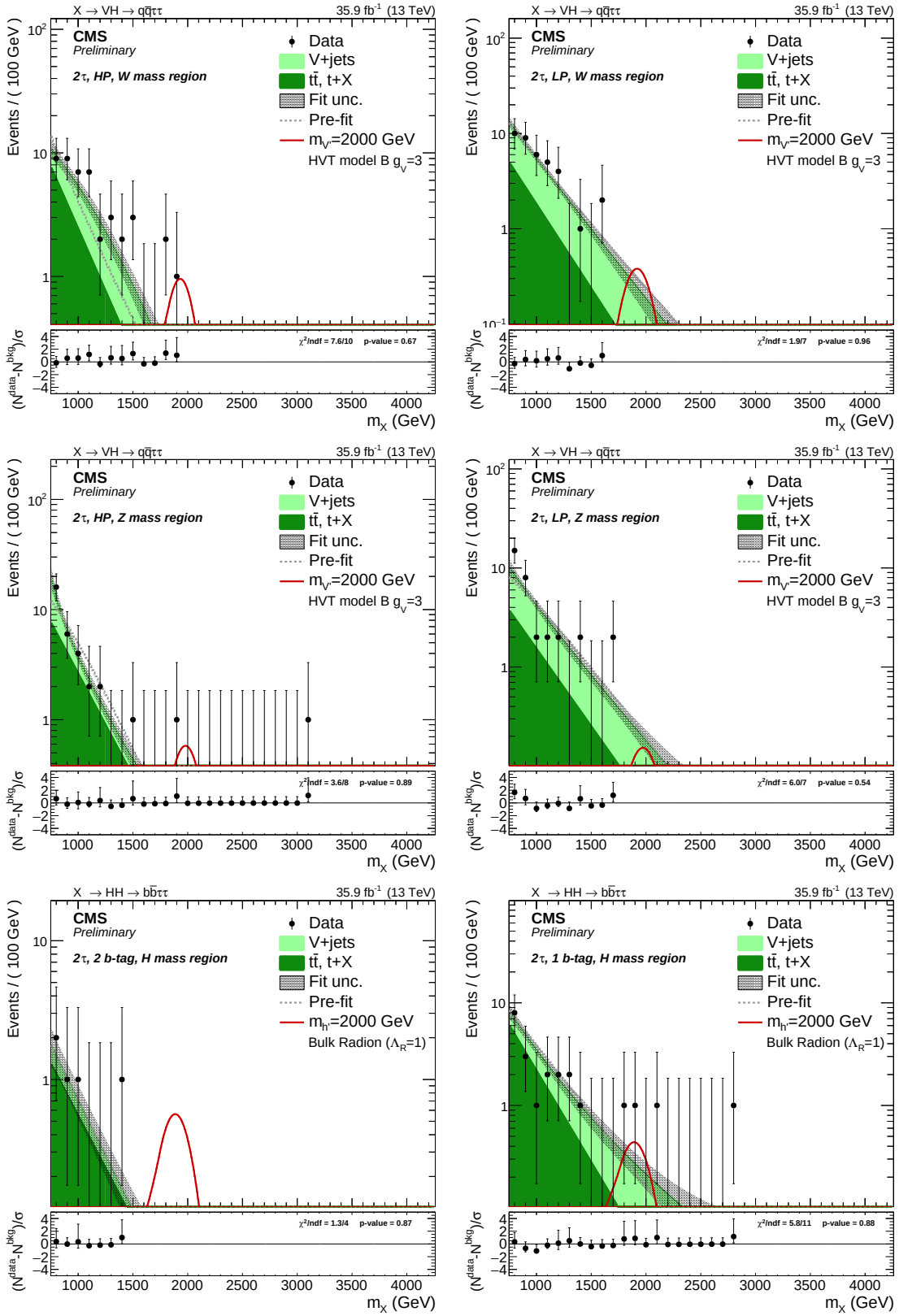

Figure 4: Data and expected background determined with the α transfer function method in the $\tau_h\tau_h$ channel: W mass window for the τ_{21} HP (upper left) and LP (upper right) categories, Z mass window for the τ_{21} HP (middle left) and LP (middle right) categories, and H mass window for the 1 b-tagged subjet (lower left) and 2 b-tagged subjets (lower right) categories. Signal contributions are also shown assuming the benchmark scenario B of the HVT model for the V′ and Λ_R=1 for the radion, each with a mass of 2 TeV.

8 Results

Results are obtained from a combined fit of the signal and background to the data of the resonance mass distribution, based on a profile likelihood where systematic uncertainties are considered as nuisance parameters and profiled in the statistical interpretation [58, 59]. The background-only hypothesis is tested against the signal hypothesis simultaneously in the various categories. With no evidence of significant deviations from the background expectation, 95% confidence level (CL) upper limits are determined for the signal using the asymptotic frequentist method [58, 60, 61]. Limits are derived on the production cross section times branching ratio for a heavy resonance (X) for the decays X→ WH, ZH or HH ($\sigma_{95\%}\times$ BR (X $\rightarrow$ WH/ ZH/ HH)). For the WH and ZH final states, a spin of 1 is considered for X, while for the HH final state, spins of 0 and 2 are considered. The limits, assuming the signal has a narrow width, much less than the experimental resonance mass resolution of around 7%, are reported in Figs. 5–6. For the WH and ZH final states, the W and Z mass regions are combined because there are contributions of both signals to the two mass regions.

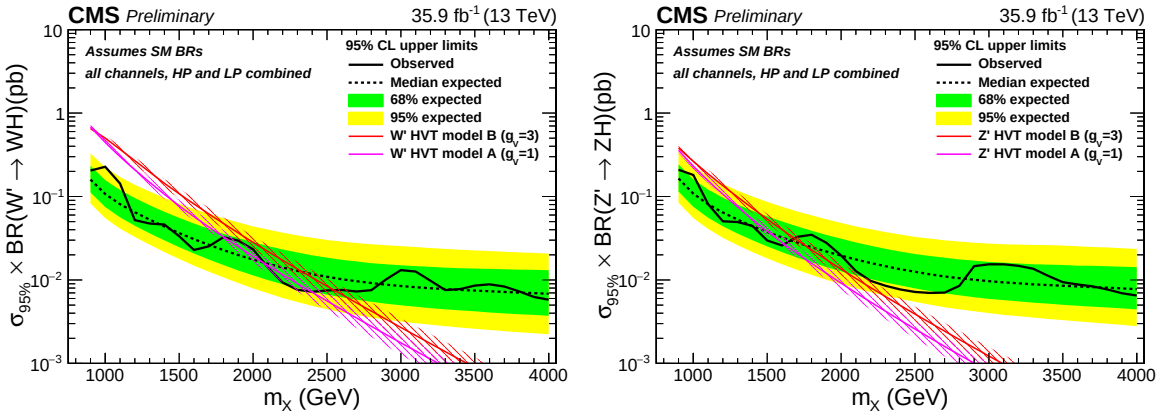

Figure 5: Observed 95% CL upper limits on $\sigma\times$BR(X→WH) (left) and $\sigma\times$BR(Z→ZH) (right). Expected limits are shown with 1 and 2σ uncertainty bands. The $\ell\tau_h$ and $\tau_h\tau_h$ final states, HP and LP τ_{21} categories, and W and Z mass signal regions are combined.

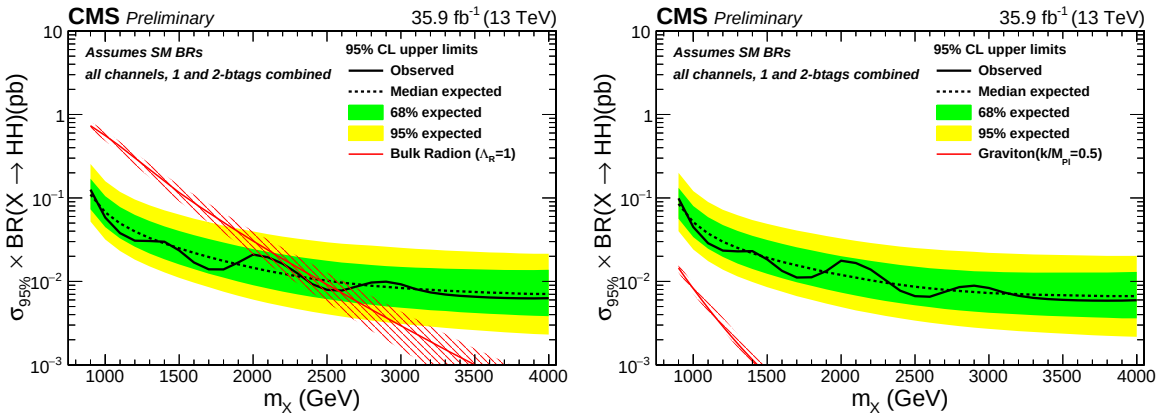

Figure 6: Observed 95% CL upper limits on $\sigma\times$BR(X(spin-0)→HH) (left) and $\sigma\times$BR(X(spin-2)→HH) (right). Expected limits are shown with 1 and 2σ uncertainty bands. The $\ell\tau_h$ and $\tau_h\tau_h$ final states, and 1 and 2 sub-jet b-tag categories are combined.

For a spin-1 signal, the results are interpreted in the context of the simplified HVT model with heavy vector bosons, which is parametrized in terms of a new interaction of strength g_V, the

coupling to the H boson or the longitudinally-polarized SM vector boson c_H, and the coupling to fermions c_F.

The prediction from the models is superimposed on the exclusion limits in Fig. 6 (left) assuming $\Lambda_R = 1$ TeV. In this scenario, a radion resonance with mass lower than 2.5 TeV is excluded at 95% CL. A W′(Z′) resonance of mass lower than 2.3 TeV (1.7 TeV) is excluded at 95% CL in the HVT benchmark model B. The HVT benchmark model A is also reported for completeness. In the mass-degenerate spin-1 triplet hypothesis, the expected and observed limits on the V′ resonance are shown in Fig. 7 (left).

The exclusion limit shown in Fig. 7 (left) can be interpreted as a limit in the space of the HVT model parameters $[g_V c_H, g^2 c_F/g_V]$. Combining all channels, the excluded region in such a parameter space for narrow resonances is shown in Fig. 7 (right). The region of parameter space where the natural resonance width is larger than the typical experimental resolution of 7%, for which the narrow width assumption is not valid, is shaded.

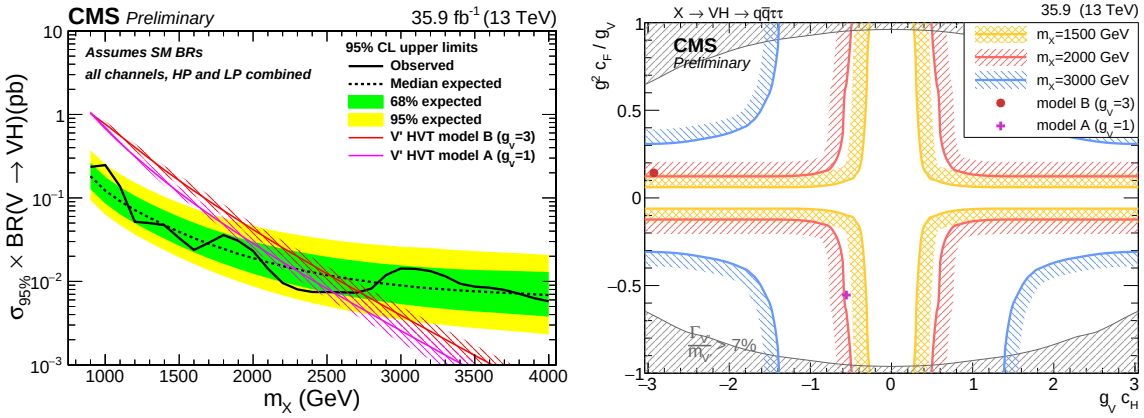

Figure 7: Expected (with $\pm 1(2)\sigma$ bands) and observed 95% CL upper limit on $\sigma \times$BR(X→VH) (left) in the $\ell\tau_h$ and $\tau_h\tau_h$, τ_{21} HP and LP categories, with W and Z mass signal regions combined. Observed exclusion limit (right) in the space of the HVT model parameters $[g_V c_H, g^2 c_F/g_V]$, described in the text, for three different mass hypotheses (1.5, 2, and 3 TeV). The region of parameter space where the natural resonance width is larger than the typical experimental resolution of 7%, for which the narrow width assumption is not valid, is shaded in grey.

9 Summary

A search has been conducted for heavy resonances, with masses between 900 GeV and 4 TeV, and which couple more strongly to bosons than fermions. The heavy particle is searched for in final states with two bosons: one of which is a W, Z, or H boson that decays hadronically; while the other is a Higgs boson that decays to a pair of tau leptons. The analyzed data are collected by the CMS experiment at $\sqrt{s} = 13$ TeV during 2016 operations, corresponding to an integrated luminosity of 35.9 fb^{-1}. Depending on the resonance mass, expected upper limits on the production cross section times branching ratios to WH, ZH, and HH, for spin-1, spin-0, and spin-2 resonances are set between 250 and 6 fb.

References

[1] W. D. Goldberger and M. B. Wise, "Modulus stabilization with bulk fields", *Phys. Rev. Lett.* **83** (1999) 4922, doi:10.1103/PhysRevLett.83.4922, arXiv:hep-ph/9907447.

[2] O. DeWolfe, D. Z. Freedman, S. S. Gubser, and A. Karch, "Modeling the fifth-dimension with scalars and gravity", *Phys. Rev. D* **62** (2000) 046008, doi:10.1103/PhysRevD.62.046008, arXiv:hep-th/9909134.

[3] C. Csaki, M. Graesser, L. Randall, and J. Terning, "Cosmology of brane models with radion stabilization", *Phys. Rev. D* **62** (2000) 045015, doi:10.1103/PhysRevD.62.045015, arXiv:hep-ph/9911406.

[4] L. Randall and R. Sundrum, "A large mass hierarchy from a small extra dimension", *Phys. Rev. Lett.* **83** (1999) 3370, doi:10.1103/PhysRevLett.83.3370, arXiv:hep-ph/9905221.

[5] L. Randall and R. Sundrum, "An alternative to compactification", *Phys. Rev. Lett.* **83** (1999) 4690, doi:10.1103/PhysRevLett.83.4690, arXiv:hep-th/9906064.

[6] K. Agashe, H. Davoudiasl, G. Perez, and A. Soni, "Warped Gravitons at the LHC and Beyond", *Phys. Rev. D* **76** (2007) 036006, doi:10.1103/PhysRevD.76.036006, arXiv:hep-ph/0701186.

[7] A. L. Fitzpatrick, J. Kaplan, L. Randall, and L.-T. Wang, "Searching for the Kaluza-Klein Graviton in Bulk RS Models", *JHEP* **09** (2007) 013, doi:10.1088/1126-6708/2007/09/013, arXiv:hep-ph/0701150.

[8] O. Antipin, D. Atwood, and A. Soni, "Search for RS gravitons via W_L W_L decays", *Phys. Lett. B* **666** (2008) 155, doi:10.1016/j.physletb.2008.07.009, arXiv:0711.3175.

[9] B. Bellazzini, C. Csáki, and J. Serra, "Composite Higgses", *Eur. Phys. J. C* **74** (2014) 2766, doi:10.1140/epjc/s10052-014-2766-x, arXiv:1401.2457.

[10] R. Contino, D. Marzocca, D. Pappadopulo, and R. Rattazzi, "On the effect of resonances in composite Higgs phenomenology", *JHEP* **10** (2011) 081, doi:10.1007/JHEP10(2011)081, arXiv:1109.1570.

[11] D. Marzocca, M. Serone, and J. Shu, "General composite Higgs models", *JHEP* **08** (2012) 013, doi:10.1007/JHEP08(2012)013, arXiv:1205.0770.

[12] D. Greco and D. Liu, "Hunting composite vector resonances at the LHC: naturalness facing data", *JHEP* **12** (2014) 126, doi:10.1007/JHEP12(2014)126, arXiv:1410.2883.

[13] M. Schmaltz and D. Tucker-Smith, "Little Higgs review", *Ann. Rev. Nucl. Part. Sci.* **55** (2005) 229, doi:10.1146/annurev.nucl.55.090704.151502, arXiv:hep-ph/0502182.

[14] N. Arkani-Hamed, A. Cohen, E. Katz, and A. Nelson, "The Littlest Higgs", *JHEP* **07** (2002) 034, doi:10.1088/1126-6708/2002/07/034, arXiv:hep-ph/0206021.

[15] G. Altarelli, B. Mele, and M. Ruiz-Altaba, "Searching for new heavy vector bosons in $p\bar{p}$ colliders", *Z. Phys. C* **45** (1989) 109, doi:10.1007/BF01556677.

[16] D. Pappadopulo, A. Thamm, R. Torre, and A. Wulzer, "Heavy Vector Triplets: Bridging Theory and Data", *JHEP* **09** (2014) 060, doi:10.1007/JHEP09(2014)060, arXiv:1402.4431.

[17] M. Gouzevitch et al., "Scale-invariant resonance tagging in multijet events and new physics in Higgs pair production", *JHEP* **07** (2013) 148, doi:10.1007/JHEP07(2013)148, arXiv:1303.6636.

[18] ATLAS Collaboration, "Search for new resonances decaying to a W or Z boson and a Higgs boson in the $\ell^+\ell^- b\bar{b}$, $\ell\nu b\bar{b}$, and $\nu\bar{\nu}b\bar{b}$ channels with pp collisions at $\sqrt{s} = 13$ TeV with the ATLAS detector", *Phys. Lett. B* **765** (2017) 32, doi:10.1016/j.physletb.2016.11.045, arXiv:1607.05621.

[19] ATLAS Collaboration, "Searches for heavy diboson resonances in pp collisions at $\sqrt{s} = 13$ TeV with the ATLAS detector", *JHEP* **09** (2016) 173, doi:10.1007/JHEP09(2016)173, arXiv:1606.04833.

[20] CMS Collaboration, "Search for new resonances decaying via WZ to leptons in proton-proton collisions at $\sqrt{s} = 8$ TeV", *Phys. Lett. B* **740** (2015) 83, doi:10.1016/j.physletb.2014.11.026, arXiv:1407.3476.

[21] CMS Collaboration, "Search for massive resonances decaying into pairs of boosted bosons in semi-leptonic final states at $\sqrt{s} = 8$ TeV", *JHEP* **08** (2014) 174, doi:10.1007/JHEP08(2014)174, arXiv:1405.3447.

[22] CMS Collaboration, "Search for massive resonances in dijet systems containing jets tagged as W or Z boson decays in pp collisions at $\sqrt{s}$ = 8 TeV", *JHEP* **08** (2014) 173, doi:10.1007/JHEP08(2014)173, arXiv:1405.1994.

[23] CMS Collaboration, "Search for massive WH resonances decaying into the $\ell\nu\mathrm{b\bar{b}}$ final state at $\sqrt{s} = 8$ TeV", *Eur. Phys. J. C* **76** (2016) 237, doi:10.1140/epjc/s10052-016-4067-z, arXiv:1601.06431.

[24] CMS Collaboration, "Search for a massive resonance decaying into a Higgs boson and a W or Z boson in hadronic final states in proton-proton collisions at $\sqrt{s} = 8$ TeV", *JHEP* **02** (2016) 145, doi:10.1007/JHEP02(2016)145, arXiv:1506.01443.

[25] CMS Collaboration, "Search for Narrow High-Mass Resonances in Proton-Proton Collisions at $\sqrt{s}$ = 8 TeV Decaying to a Z and a Higgs Boson", *Phys. Lett. B* **748** (2015) 255, doi:10.1016/j.physletb.2015.07.011, arXiv:1502.04994.

[26] ATLAS Collaboration, "Search for high-mass diboson resonances with boson-tagged jets in proton-proton collisions at $\sqrt{s} = 8$ TeV with the ATLAS detector", *JHEP* **12** (2015) 055, doi:10.1007/JHEP12(2015)055, arXiv:1506.00962.

[27] ATLAS Collaboration, "Search for production of WW/WZ resonances decaying to a lepton, neutrino and jets in pp collisions at $\sqrt{s} = 8$ TeV with the ATLAS detector", *Eur. Phys. J. C* **75** (2015) 209, doi:10.1140/epjc/s10052-015-3593-4, 10.1140/epjc/s10052-015-3425-6, arXiv:1503.04677. [Erratum: *Eur. Phys. J. C* **75** *(2015) 370*].

[28] ATLAS Collaboration, "Search for WZ resonances in the fully leptonic channel using pp collisions at $\sqrt{s}$ = 8 TeV with the ATLAS detector", *Phys. Lett. B* **737** (2014) 223, doi:10.1016/j.physletb.2014.08.039, arXiv:1406.4456.

[29] ATLAS Collaboration, "Search for a new resonance decaying to a W or Z boson and a Higgs boson in the $\ell\ell/\ell\nu/\nu\nu + b\bar{b}$ final states with the ATLAS detector", *Eur. Phys. J. C* **75** (2015) 263, doi:10.1140/epjc/s10052-015-3474-x, arXiv:1503.08089.

[30] F. Dias et al., "Combination of Run-1 Exotic Searches in Diboson Final States at the LHC", *JHEP* **04** (2016) doi:10.1007/JHEP04(2016)155, arXiv:1512.03371.

[31] CMS Collaboration, "The CMS trigger system", *JINST* **12** (2017) P01020, doi:10.1088/1748-0221/12/01/P01020, arXiv:1609.02366.

[32] CMS Collaboration, "The CMS experiment at the CERN LHC", *JINST* **3** (2008) S08004, doi:10.1088/1748-0221/3/08/S08004.

[33] J. Alwall et al., "MadGraph 5 : Going Beyond", *JHEP* **06** (2011) 128, doi:10.1007/JHEP06(2011)128, arXiv:1106.0522.

[34] P. Nason, "A new method for combining NLO QCD with shower Monte Carlo algorithms", *JHEP* **11** (2004) 040, doi:10.1088/1126-6708/2004/11/040, arXiv:hep-ph/0409146.

[35] S. Frixione, P. Nason, and C. Oleari, "Matching NLO QCD computations with Parton Shower simulations: the POWHEG method", *JHEP* **11** (2007) 070, doi:10.1088/1126-6708/2007/11/070, arXiv:0709.2092.

[36] S. Alioli, P. Nason, C. Oleari, and E. Re, "A general framework for implementing NLO calculations in shower Monte Carlo programs: the POWHEG BOX", *JHEP* **06** (2010) 043, doi:10.1007/JHEP06(2010)043, arXiv:1002.2581.

[37] S. Alioli, S.-O. Moch, and P. Uwer, "Hadronic top-quark pair-production with one jet and parton showering", *JHEP* **01** (2012) 137, doi:10.1007/JHEP01(2012)137, arXiv:1110.5251.

[38] T. Sjöstrand, S. Mrenna, and P. Z. Skands, "PYTHIA 6.4 Physics and Manual", *JHEP* **05** (2006) 026, doi:10.1088/1126-6708/2006/05/026, arXiv:hep-ph/0603175.

[39] S. Jadach, J. H. Kuhn, and Z. Was, "TAUOLA: A Library of Monte Carlo programs to simulate decays of polarized tau leptons", *Comput. Phys. Commun.* **64** (1990) 275, doi:10.1016/0010-4655(91)90038-M.

[40] GEANT4 Collaboration, "GEANT4: A simulation toolkit", *Nucl. Instrum. Meth. A* **506** (2003) 250, doi:10.1016/S0168-9002(03)01368-8.

[41] CMS Collaboration, "Particle-flow reconstruction and global event description with the CMS detector", *JINST* **12** (2017), no. 10, P10003, doi:10.1088/1748-0221/12/10/P10003, arXiv:1706.04965.

[42] M. Cacciari, G. P. Salam, and G. Soyez, "The Anti-k(t) jet clustering algorithm", *JHEP* **04** (2008) 063, doi:10.1088/1126-6708/2008/04/063, arXiv:0802.1189.

[43] M. Cacciari, G. P. Salam, and G. Soyez, "FastJet User Manual", *Eur. Phys. J. C* **72** (2012) 1896, doi:10.1140/epjc/s10052-012-1896-2, arXiv:1111.6097.

[44] D. Bertolini, P. Harris, M. Low, and N. Tran, "Pileup Per Particle Identification", *JHEP* **10** (2014) 059, doi:10.1007/JHEP10(2014)059, arXiv:1407.6013.

[45] M. Dasgupta, A. Fregoso, S. Marzani, and G. P. Salam, "Towards an understanding of jet substructure", *JHEP* **09** (2013) 029, doi:10.1007/JHEP09(2013)029, arXiv:1307.0007.

[46] A. J. Larkoski, S. Marzani, G. Soyez, and J. Thaler, "Soft drop", *JHEP* **05** (2014) 146, doi:10.1007/JHEP05(2014)146, arXiv:1402.2657.

[47] J. Thaler and K. Van Tilburg, "Identifying Boosted Objects with N-subjettiness", *JHEP* **03** (2011) 015, doi:10.1007/JHEP03(2011)015, arXiv:1011.2268.

[48] CMS Collaboration, "Jet algorithms performance in 13 TeV data", CMS Physics Analysis Summary CMS-PAS-JME-16-003, CERN, 2017.

[49] CMS Collaboration, "Identification of b-quark jets with the CMS experiment", *JINST* **8** (2013) P04013, doi:10.1088/1748-0221/8/04/P04013, arXiv:1211.4462.

[50] CMS Collaboration, "Identification of b quark jets at the CMS Experiment in the LHC Run 2", CMS Physics Analysis Summary CMS-PAS-BTV-15-001, CERN, 2016.

[51] CMS Collaboration, "Tau identification in boosted topologies", CMS Detector Performance Summary CMS-DP-2016-038, Jul, 2016.

[52] M. Wobisch and T. Wengler, "Hadronization corrections to jet cross-sections in deep inelastic scattering", in *Monte Carlo generators for HERA physics. Proceedings, Workshop, Hamburg, Germany, 1998-1999*, p. 270. 1998. arXiv:hep-ph/9907280.

[53] CMS Collaboration, "Performance of tau-lepton reconstruction and identification in CMS", *JINST* **7** (2012) P01001, doi:10.1088/1748-0221/7/01/P01001, arXiv:1109.6034.

[54] CMS Collaboration, "Performance of electron reconstruction and selection with the CMS detector in proton-proton collisions at $\sqrt{s} = 8$ TeV", *JINST* **10** (2015) P06005, doi:10.1088/1748-0221/10/06/P06005, arXiv:1502.02701.

[55] CMS Collaboration, "Performance of CMS muon reconstruction in pp collision events at $\sqrt{s} = 7$ TeV", *JINST* **7** (2012) P10002, doi:10.1088/1748-0221/7/10/P10002, arXiv:1206.4071.

[56] CMS Collaboration, "Search for Neutral MSSM Higgs Bosons Decaying to Tau Pairs in pp Collisions at $\sqrt{s} = 7$ TeV", *Phys. Rev. Lett.* **106** (2011) 231801, doi:10.1103/PhysRevLett.106.231801, arXiv:1104.1619.

[57] M. Bahr et al., "Herwig++ Physics and Manual", *Eur. Phys. J. C* **58** (2008) 639, doi:10.1140/epjc/s10052-008-0798-9, arXiv:0803.0883.

[58] A. L. Read, "Presentation of search results: the CL_s technique", *J. Phys. G* **28** (2002) 2693, doi:10.1088/0954-3899/28/10/313.

[59] G. Cowan, K. Cranmer, E. Gross, and O. Vitells, "Asymptotic formulae for likelihood-based tests of new physics", *Eur. Phys. J. C* **71** (2011) 1554, doi:10.1140/epjc/s10052-011-1554-0, 10.1140/epjc/s10052-013-2501-z, arXiv:1007.1727. [Erratum: *Eur. Phys. J. C* **73** *(2013) 2501*].

[60] T. Junk, "Confidence level computation for combining searches with small statistics", *Nucl. Instrum. Meth. A* **434** (1999) 435, doi:10.1016/S0168-9002(99)00498-2, arXiv:hep-ex/9902006.

[61] ATLAS and CMS Collaborations, LHC Higgs Combination Group, "Procedure for the LHC Higgs boson search combination in Summer 2011", Technical Report ATL-PHYS-PUB-2011-11, CMS-NOTE-2011-005, 2011.